J. Phys. Chem. A **2005,** *109,* 2971−2977

On the Extent of Intramolecular Hydrogen Bonding in Gas-Phase and Hydrated 1,2-Ethanediol

Deborah L. Crittenden,* Keiran C. Thompson, and Meredith J. T. Jordan

School of Chemistry, University of Sydney, NSW, Australia 2006

Received: October 19, 2004; In Final Form: January 23, 2005

We investigate the quantum dynamical nature of hydrogen bonding in 1,2-ethanediol and monohydrated 1,2-ethanediol using different levels of *ab initio* theory. Global full-dimensional potential energy surfaces were constructed from PW91/cc-pVDZ, B3LYP/cc-pVDZ, and MP2/cc-pVDZ *ab initio* data for gas-phase and monohydrated 1,2-ethanediol, using a modified Shepard interpolation scheme. Zero-point energies and nuclear vibrational wave functions were calculated on these surfaces using the quantum diffusion Monte Carlo algorithm. The nature of intra- and intermolecular hydrogen bonding in these molecules was investigated by considering a ground-state nuclear vibrational wavefunction with reduced complete nuclear permutation and inversion (CNPI) symmetry. Separate wavefunction histograms were determined from the ground-state nuclear vibrational wavefunction by projection into bondlength coordinates. The O−H and O−O wavefunction histograms and vibrationally averaged distances were then used to probe the extent of intra- and intermolecular hydrogen bonding. From these data, we conclude that gas-phase ethanediol may possess a weak hydrogen bond, with a relatively short O−O distance but no detectable proton delocalization. Monohydrated ethanediol was found to exhibit no intramolecular hydrogen bonding but instead possessed two intermolecular hydrogen bonds, indicated by both shortening of the O−O distance and significant proton delocalization. The degree of proton delocalization and shortening of the vibrationally averaged O−O distance was found to be dependent on the *ab initio* method used to generate the potential energy surface (PES) data set.

Introduction

As a simple model for biologically significant polyhydroxylated molecules such as sugars and carbohydrates, 1,2-ethanediol (Figure 1a) has been the subject of intensive theoretical[1−25] and experimental[2,4,9,26−36] investigation.

A large number of *ab initio* studies have been carried out on gas-phase ethanediol,[1−10,12−21,24,25] ranging from HF calculations with small split-valence basis sets and partially optimized geometries[1−4] to G2(MP2) calculations with fully optimized MP2/6-31+G* geometries.[24] These studies have established that, provided that sufficiently large (at least valence double-ζ) basis sets are used with a method that includes some correlation correction (at least density functional theory), all 10 symmetry-distinct rotamers obtained by rotation about the H−O−C−C and O−C−C−O dihedrals (Figure 2) are local minima on the gas-phase ethanediol potential energy surface (PES). All of these investigations found that the relative energies of all 10 rotamers lie within 14.6 kJ/mol, with the tGg′ isomer being the lowest in energy by around 1.7 kJ/mol from the next lowest energy isomer, gGg′.

These theoretical results are in good agreement with experimental microwave spectroscopy,[24,27,33,34,36] electron diffraction,[26] and infrared (IR) spectroscopy[29] on gas-phase ethanediol. These studies all agree that tGg′ is the predominant conformer, although the IR results suggest that the gGg′ isomer may also be accessible through zero-point and thermal motion.

A smaller number of theoretical[8,10,11,13,15,22,23] and experimental[28,30−32] studies have been carried out on solvated 1,2-ethanediol. A number of approaches have been utilized to model the effect of solvation on 1,2-ethanediol, from determination of low-energy conformations of the monohydrated solute[23] to classical molecular dynamics simulations incorporating 195 water molecules surrounding the solute.[11] The results obtained will be briefly summarized below. For further details of each method, we refer the reader to the papers referenced here and the references cited therein.

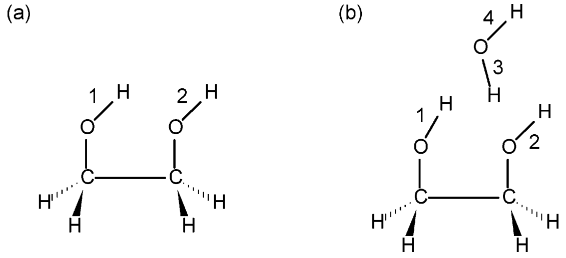

Figure 1. 1,2-Ethanediol and 1,2-ethanediol monohydrate, with the O−H bonds labeled.

The simplest solvation model, monohydrated 1,2-ethanediol (Figure 1b), was studied by Manivet et al.[23] At the MP2/6-31G* level of theory, it was found that the most stable conformation involved intermolecular hydrogen bonding between both hydroxide groups of the ethanediol molecule and the bridging water. The configurations with only one hydrogen bond between the ethanediol and the water molecule were 8.4 kJ/mol higher in energy. According to the polarizable continuum solvation model used by both Alagona et al.[10] and Cabral,[22] using MP2/4-31G* and BLYP/6-31G**, respectively, the tGg′ and gGg′ conformers were found to be most stable in solution, followed by the g′Gg′ conformer and then the tTt conformer. Explicit solvent simulations have been performed by Nagy et

---

* Corresponding author. E-mail: m.jordan@chem.usyd.edu.au.

10.1021/jp045233h CCC: $30.25

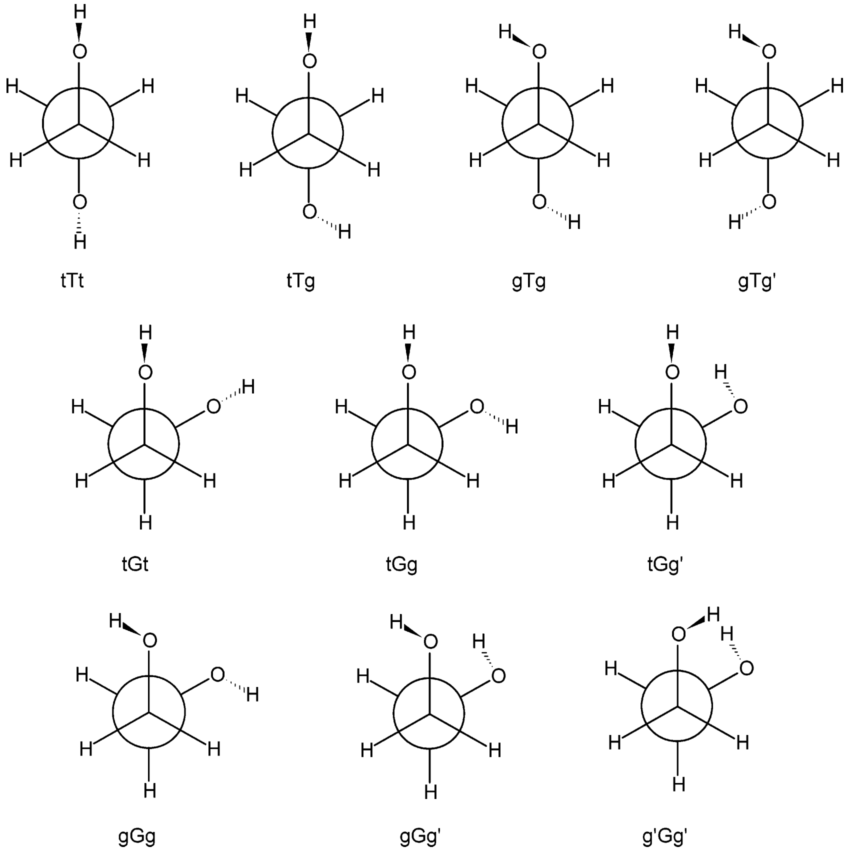

Figure 2. The 10 symmetry-distinct rotamers of 1,2-ethanediol, depicted as Newman projections. The two lowest energy configurations in the gas phase are tGg′ and gGg′.

al.[8,13] and Hooft et al.[11] The approach taken by Nagy et al. was to optimize the geometries of four ethanediol conformers (tGg′, gGg′, g′Gg′, and tTt) in the gas phase at HF/6-31G* and then combine the MP2/6-31G* internal energy at each geometry with the solvation energy determined from a Monte Carlo simulation using the OPLS force field with the TIP4P intermolecular potential. Hooft et al. employed a molecular dynamics approach, allowing for nuclear motion of the solute within the solvent model and hence considering all possible ethanediol conformers. This simulation used a molecular mechanics method to describe the ethanediol molecule with a simple point charge (SPC) water model. Both studies found that the gauche and trans isomers are likely to coexist in aqueous solution, although Nagy et al. predicted a 99:1 gauche-to-trans ratio, while Hooft et al. predicted 67:33 for the same quantity. Adopting a different approach, Cramer and Truhlar[15] used the semiempirical-based AM1-SMX and PM3-SMX solvation models with MP2/cc-pVDZ internal energies. Similar to Monte Carlo and molecular dynamics studies, it was found that both gauche and trans isomers of 1,2-ethanediol are likely to coexist in a ratio of 75:25. These theoretical predictions are consistent with nuclear magnetic resonance (NMR) studies of 1,2-ethanediol in aqueous solution,[30] which predict a gauche-to-trans ratio of 88:12.

Although 1,2-ethanediol has been the subject of intense theoretical investigation, we are not currently aware of any studies that have been carried out to determine the *quantum* motion of the nuclei for either the gas-phase or solvated system. Quantum nuclear motion becomes important if there are a number of low-lying local minima on the global potential energy surface that have low barriers to interconversion. In these cases, a number of states may be accessible through zero-point and thermal motion. An example of such a system is solvated ethanediol, where the tGg′ and gGg′ conformers are predicted to be approximately isoenergetic in aqueous solution, and delocalization of the nuclear vibrational wavefunction over both the conformers may occur. Quantum nuclear motion is also important in predicting the behavior of smaller, lighter atoms, such as hydrogen. Examination of the nuclear motion of protons may provide a probe of the extent of hydrogen bonding in a molecule or complex. Previous studies have sought to characterize the nature of intramolecular hydrogen bonding in 1,2-ethanediol on the basis of geometrical, energetic, and electron density topological data. From the geometrical and energetic studies that have been carried out,[1−10,12−21,24] the stabilization of the two gauche conformers tGg′ and gGg′ and the elongation of the bridging O−H have been taken as evidence of the presence of an intramolecular hydrogen bond in 1,2-ethanediol. More recently, however, a number of electron density topological studies[25,37] have concluded that 1,2-ethanediol does not possess an intramolecular hydrogen bond, according to the criteria for bonding defined by Popelier.[38] As yet, however, no definitive criterion has been established for characterizing the presence, nature, and strength of intramolecular hydrogen bonds. We propose that examining the extent of proton delocalization in the nuclear vibrational wavefunction may provide a solution to this problem. Therefore, in this study, we set out to determine the quantum motion of the nuclei of gas-phase and monohydrated 1,2-ethanediol. We describe how the nuclear vibrational wavefunction can be used to probe hydrogen bonding and to answer the following questions:

(1) Does 1,2-ethanediol have an intramolecular hydrogen bond?

(2) How is the intramolecular 1,2-ethanediol bonding changed upon the addition of a water molecule? That is, does monohydrated 1,2-ethanediol have an intramolecular hydrogen bond, only intermolecular hydrogen bonds, or both?

TABLE 1: Parameters Used in Quantum Diffusion Monte Carlo Simulations

	ethanediol		monohydrated ethandiol	
parameter	sampling	convergence	sampling	convergence
number of replicas	1200	900	1000	1000
maximum initial displacement from equilibrium (Bohr)	0.5	0.5	0.5	0.5
number of time steps, equilibration phase	1000	50 000	1000	50 000
number of time steps, production phase	4000	50 000	4000	50 000
step size (a.u.)	0.1	1.0	0.1	1.0
number of descendant weighting generations	N/A	40	N/A	40
number of time steps, descendant weighting	N/A	20 000	N/A	20 000

(3) What is the effect of using different levels of *ab initio* theory to construct the global potential energy surface (PES) on the nuclear vibrational wavefunction, in particular, on the extent and nature of hydrogen bonding?

Computational Methods

The methods used in this work are based on constructing an interpolated potential energy surface from *ab initio* data and calculating quantum observables using the quantum diffusion Monte Carlo (QDMC) algorithm. Each of these steps will be explained in further detail below.

The calculations reported here were carried out on the computing facilities of the School of Chemistry at the University of Sydney and at the Australian Partnership for Advanced Computing (APAC) National Facility.

PES Interpolation. The details of the modified Shepard interpolation scheme developed by Collins and co-workers[39−41] have been previously reported. We refer the reader to a recent review for further details[42] and summarize the salient features of the scheme here. Briefly, the potential energy at any molecular configuration is expressed as a weighted sum of second-order Taylor polynomials about data points in a PES data set. The energy and derivative data required for the Taylor polynomial expansions are obtained from *ab initio* electronic structure calculations. The PES is constructed in inverse bondlength coordinates and is designed to be invariant to complete nuclear permutation and inversion (CNPI) symmetry. A key feature of the interpolation scheme is that the PES is "grown" by iterative improvement of the PES data set. Each iteration consists of a dynamics simulation to explore configuration space, the selection of new data points from configurations accessed by the dynamics simulation, and the calculation of energetic and derivative data at the selected molecular configurations. This cycle is continued until the observable of interest ceases to change upon the addition of further data.

For the gas-phase ethanediol molecule, the initial data set was defined by six stationary points on the global PES, with the local minima corresponding to the conformers tGg′, tGt, and tTt and the transition states corresponding to tGg′ isomerization, tGt isomerization, and conversion of tTt to tGt. We considered each of these configurations to possess 192 CNPI symmetry equivalent structures, defined by permutation of the two equivalent carbon atoms, the two equivalent oxygen atoms, the four equivalent carbon-bound hydrogen atoms, and the two equivalent oxygen-bound hydrogen atoms. For the monohydrated ethanediol molecule, the initial data set was defined by a collection of five approximately isoenergetic local minima. The permutation symmetry group was defined by considering all atoms distinct except the two hydrogen atoms bound to the water molecule, which are considered equivalent, and the two sets of two carbon−hydrogen atoms, where the hydrogen atoms in each set are considered equivalent. Although this CNP group is minimal, it is expected to contain most of the feasible permutations encountered during the QDMC simulation, as the atomic displacements are small and atomic rearrangements are not expected to occur. QDMC simulations were then used to sample configuration space. The details of these QDMC simulations are given in the QDMC section below. From the configurations accessed during the QDMC simulation, an alternating *h*-weight[39] and root-mean-squared (rms) deviation[43] scheme was used to select molecular configurations to become new data points. The details of the *ab initio* calculations performed at these geometries are given in the *ab initio* section below.

QDMC Calculations. The fully anharmonic zero-point energy and nuclear vibrational wavefunction were determined using the quantum diffusion Monte Carlo algorithm[44−46] with energies calculated from the interpolated PES. The parameters used for both the sampling and convergence QDMC simulations are given in Table 1.

Convergence of the ethanediol PES was monitored, in terms of the zero-point energy and nuclear vibrational wavefunction, after 1, 10, 25, 50, 75, and 100 data points had been added to the PES. Convergence of the monohydrated ethanediol PES was monitored after the addition of 1, 10, 25, 50, 75, and 100 data points to the PES. Ten independent simulation runs were carried out, and the zero-point energy reported here was calculated as the average of the 10 values obtained. The reported uncertainty in the zero-point energy is twice the standard error of the mean, $2\sigma/\sqrt{N}$, where σ is the standard deviation of the 10 energy values and $N = 10$.

Wavefunction histograms were obtained by binning the interatomic distances into 0.05 b bins for each replica at every time step of the simulation run and averaging over the 10 simulation runs. These wavefunction histograms were constructed without incorporating CNP symmetry. That is, each of the atoms that would be indistinguishable according to CNP symmetry were labeled such that all atoms and interatomic distances were artifically distinguishable. This enabled each interatomic distance to be monitored separately during the course of the QDMC simulation. To obtain physically relevant observables, it is necessary to "undo" the artificial labeling of atoms and average over CNP equivalent histograms. Vibrationally averaged internal coordinates were obtained using the descendent weighting algorithm.[46] Again, the vibrationally averaged internal coordinates were calculated without incorporating CNP symmetry, and postprocessing by averaging over CNP equivalent internal coordinates is required to yield physically relevant observables.

***Ab Initio* Calculations.** For each system, three potential energy surfaces were constructed, each using a different method for treating electron correlation, either density functional theory (DFT) using the PW91 functional,[47−51] DFT using the B3LYP functional,[52,53] or second-order many-body Møller−Plesset perturbation theory (MP2).[54] The Huzinage−Dunning correlation consistent valence double-split basis set (cc-pVDZ),[55] as implemented in the Gaussian 98 program package,[56] was used for all *ab initio* calculations. This basis set was chosen as it

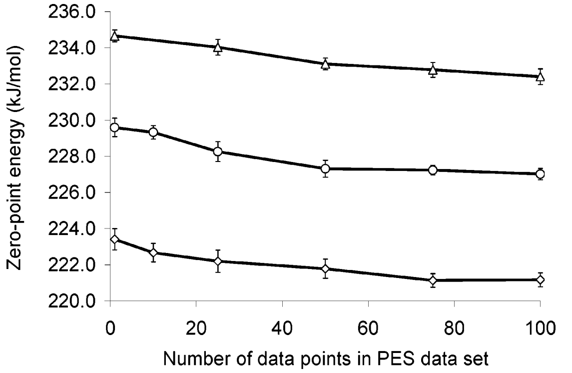

Figure 3. Convergence of zero-point vibrational energy with respect to the size of the PES data set for ethanediol gas-phase surfaces grown at PW91/cc-pVDZ (◇), B3LYP/cc-pVDZ (○), and MP2/cc-pVDZ (△).

represents an acceptable tradeoff between computational expense and chemical accuracy for this system.[24] The first and second derivatives of the energy with respect to nuclear displacement were obtained using analytic differentiation.

Results and Discussion

Gas-Phase 1,2-Ethanediol. The zero-point energy of 1,2-ethanediol as a function of the number of distinct data points that define the global PES is illustrated in Figure 3. From this figure, we observe that all three potential energy surfaces have converged with respect to quantum diffusion Monte Carlo evaluation of the ground-state energy to within ±0.5 kJ/mol by 100 data points. From this figure, we also observe that the MP2, B3LYP, and PW91 energies fall within a range of 11.2 kJ/mol, with energies in the following order:

$$\text{MP2} > \text{B3LYP} > \text{PW91}$$

As the zero-point energy depends only on the topology of the PES, these energy differences are diagnostic of differences in shape between the MP2, B3LYP, and PW91 potential energy surfaces. For a one-dimensional system, the relationship between PES topology and zero-point energy is straightforward; increasing the steepness of the walls serves to increase the zero-point energy, whereas the shallower the minima, the lower the zero-point energy. These results suggest that the MP2 surface would, relative to the B3LYP and PW91 surfaces, have either steeper walls, tighter minima, higher barriers, or some combination of the above. Similarly, the B3LYP surface would be expected to have either steeper walls, tighter minima, or higher barriers than the PW91 PES.

Each of the potential energy surfaces was found to have converged with respect to the construction of O−H wavefunction histograms from the ground-state nuclear vibrational wavefunction by the addition of 100 data points to the data set defining the PES. The superposed wavefunction histograms from the 1, 10, 25, 50, 75, and 100 data point potential energy surfaces were found to agree to within the uncertainty of the QDMC simulations, and only the wavefunction histograms calculated from the 100 data point surfaces are shown in Figure 4.

Although wavefunction histograms were constructed from the nuclear vibrational wavefunction for both O−H distances separately, we report only one O−H wavefunction histogram (Figure 4) and one vibrationally averaged O−H bond length (Table 2) for each potential energy surface, as the two wavefunction histograms were found to be identical. This implies that there is no proton delocalization in gas-phase 1,2-ethanediol to within the accuracy of our QDMC simulation. From Figure 4 and Table 2, we also observe that the B3LYP and MP2 surfaces give qualitatively similar wavefunction histograms and vibrationally averaged bond lengths, whereas the PW91 surface gives a wavefunction histogram which is shifted to longer O−H distance, giving a significantly longer average bond length. This is, however, a reflection of the fact that PW91 predicts a longer equilibrium bond length than B3LYP and MP2, rather than larger magnitude proton motion due to zero-point vibration. In fact, the magnitude of proton motion was independent of the level of *ab initio* theory used to construct the PES. In all cases, the vibrationally averaged O−H distances were found to be ~0.028 Å longer than the equilibrium distances.

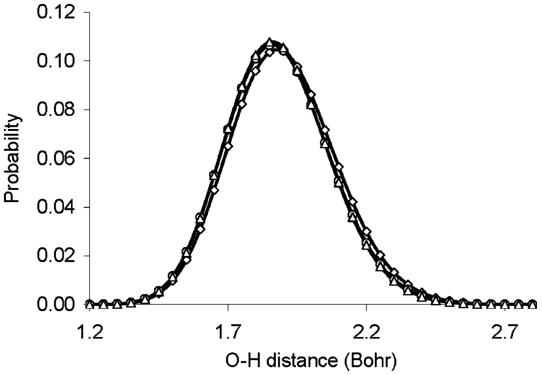

Figure 4. O−H wavefunction histograms for gas-phase ethanediol calculated from converged, 100 data point potential energy surfaces at PW91/cc-pVDZ (◇), B3LYP/cc-pVDZ (○), and MP2/cc-pVDZ (△). Only one O−H wavefunction histogram is depicted, as both were identical upon convergence. The standard error of the mean falls within the size of the data points.

TABLE 2: Equilibrium (r_0) and Vibrationally Averaged (r_{eq}) O−H Distances (Å) for Gas-Phase and Monohydrated Ethanediol[a]

	ethanediol	monohydrated ethanediol	
theory	non-H-bonded	non-H-bonded	H-bonded
PW91 r_0	1.006 ± 0.003	1.004 ± 0.003	1.027 ± 0.003
PW91 r_{eq}	0.978 ± 0.003	0.976 ± 0.001	0.996 ± 0.001
B3LYP r_0	0.996 ± 0.003	0.992 ± 0.002	1.005 ± 0.003
B3LYP r_{eq}	0.969 ± 0.002	0.968 ± 0.001	0.982 ± 0.001
MP2 r_0	0.996 ± 0.003	0.992 ± 0.002	1.002 ± 0.003
MP2 r_{eq}	0.968 ± 0.002	0.967 ± 0.001	0.977 ± 0.001

[a] Vibrationally averaged bond lengths were calculated from the converged 100 data point PW91/cc-pVDZ, B3LYP/cc-pVDZ, and MP2/cc-pVDZ potential energy surfaces.

The vibrationally averaged O−O heavy atom distance is also known to provide a probe of hydrogen-bond strength,[57] and the vibrationally averaged O−O distances for both gas-phase and monohydrated ethanediol are reported in Table 3. From this table, we observe that the intramolecular O−O distances for gas-phase ethanediol are similar to the intermolecular O−O distances for monohydrated ethanediol to within numerical uncertainty, irrespective of the level of theory used to construct the PES. At this O−O distance, monohydrated ethanediol is known to exhibit intermolecular hydrogen bonding. This implies that, with a similar O−O distance, gas-phase ethanediol will exhibit intramolecular hydrogen bonding. Overall, this evidence suggests that gas-phase ethanediol may possess a weak intramolecular hydrogen bond, although our simulation is not sensitive enough to resolve any proton delocalization.

From Table 3, we also observe that there is no clear pattern of deviation of the vibrationally averaged O−O distances from equilibrium, although in the majority of cases the vibrationally

TABLE 3: Equilibrium (r_0) and Vibrationally Averaged (r_{eq}) O−O Distances (Å) for Gas-Phase and Monohydrated Ethanediol[a]

	ethanediol	monohydrated ethanediol	
theory	intramolecular	intramolecular	intermolecular
PW91 r_0	2.694 ± 0.018	3.084 ± 0.026	2.723 ± 0.026
PW91 r_{eq}	2.728 ± 0.001	3.045 ± 0.001	2.733 ± 0.003
B3LYP r_0	2.769 ± 0.025	3.029 ± 0.027	2.789 ± 0.029
B3LYP r_{eq}	2.755 ± 0.001	3.021 ± 0.001	2.767 ± 0.002
MP2 r_0	2.683 ± 0.034	3.064 ± 0.088	2.768 ± 0.053
MP2 r_{eq}	2.746 ± 0.001	3.009 ± 0.001	2.774 ± 0.004

[a] Vibrationally averaged bond lengths were calculated from the converged 100 data point PW91/cc-pVDZ, B3LYP/cc-pVDZ, and MP2/cc-pVDZ potential energy surfaces.

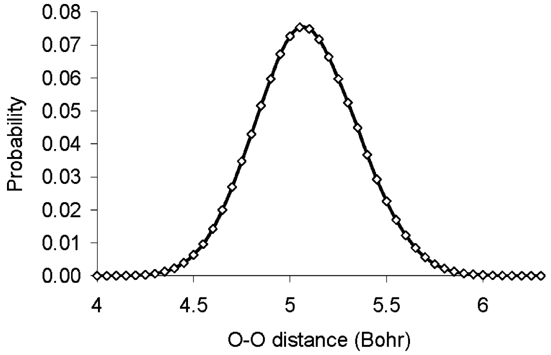

Figure 5. O−O wavefunction histogram for gas-phase ethanediol calculated from the converged, 100 data point MP2/cc-pVDZ potential energy. The standard error of the mean falls within the size of the data points.

averaged O−O distances are similar to the equilibrium distances to within numerical uncertainty. This implies that the PES is symmetric along this coordinate over the range of bond lengths accessed by the nuclear vibrational wavefunction. This is confirmed by the symmetric O−O wavefunction histogram illustrated in Figure 5. It is also interesting to note that the standard error of the mean is significantly larger for the vibrationally averaged O−O distances than the O−H distances (Tables 2 and 3), and there are two factors which account for this behavior. First, the PES is shallower along the O−O coordinate and hence larger amplitude vibrational motion is observed, with a concomitant increase in the uncertainty. From Figure 4, we observe that the O−H wavefunction histogram is delocalized over 1.2 Å, while Figure 5 shows that the O−O wavefunction histogram is delocalized over 1.7 Å. Second, the statistical error in the O−H distance can be reduced by averaging over the symmetry equivalent O−H distances, whereas gas-phase ethanediol possesses only one O−O distance.

Monohydrated 1,2-Ethanediol. The zero-point energy of monohydrated 1,2-ethanediol as a function of the number of distinct data points that define the global PES is illustrated in Figure 6. From this figure, we observe that all three potential energy surfaces have converged with respect to calculation of the ground-state energy to within ±0.75 kJ/mol by 100 data points. We also observe that the zero-point energies differ according to the *ab initio* method used to construct the PES, with the energies falling within a range of 15.4 kJ/mol. Similar to gas-phase 1,2-ethanediol, the order of the energies is the following:

$$\mathrm{MP2} > \mathrm{B3LYP} > \mathrm{PW91}$$

and similar arguments can be invoked about the topology of these potential energy surfaces.

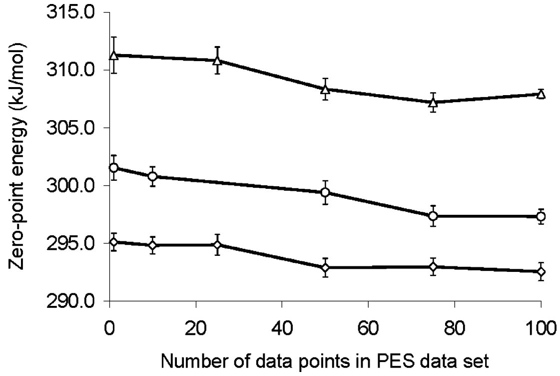

Figure 6. Convergence of zero-point vibrational energy with respect to the size of the PES data set for monohydrated ethanediol surfaces grown at PW91/cc-pVDZ (◇), B3LYP/cc-pVDZ (○), and MP2/cc-pVDZ (△).

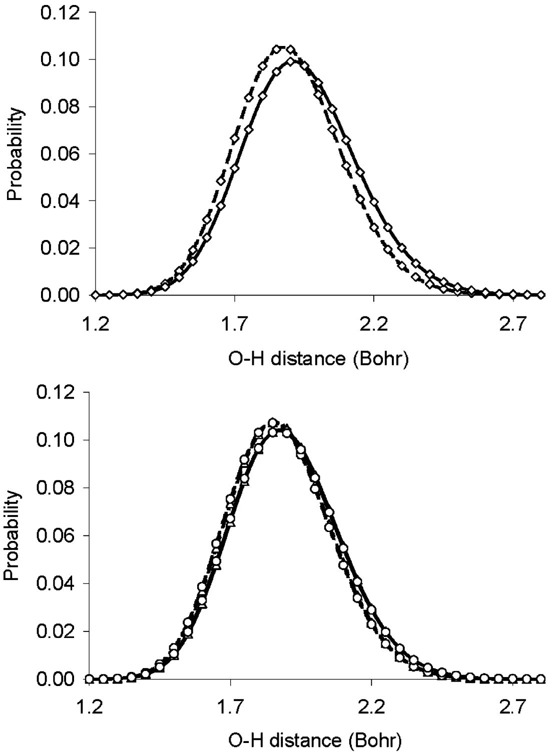

Figure 7. O−H wavefunction histograms for monohydrated ethanediol, calculated from the converged, 100 data point PW91/cc-pVDZ (◇), B3LYP/cc-pVDZ (○), and MP2/cc-pVDZ (△) potential energy surfaces. The two radial distribution functions correspond to both hydrogen-bonded (solid line) and non-hydrogen-bonded (dashed line) protons. The wavefunction histograms for the hydrogen-bonded protons were generated by averaging histograms from O−H bonds 1 and 3 (Figure 1). The wavefunction histograms for the non-hydrogen-bonded protons were generated by averaging histograms from O−H bonds 2 and 4 (Figure 1). The standard error of the mean falls within the size of the data points.

Separate O−H wavefunction histograms for all four O−H bonds in monohydrated 1,2-ethanediol were constructed from the nuclear vibrational wavefunctions calculated using the PW91, B3LYP, and MP2 potential energy surfaces. The wavefunction histograms shown in Figure 7 were calculated from data sets defined by 100 data points. One hundred data points corresponded to the minimum number of data points required to demonstrate convergence of the PES with respect to the construction of O−H wavefunction histograms, as illustrated in Figure 8. Vibrationally averaged O−H and O−O distances were subsequently calculated from these converged

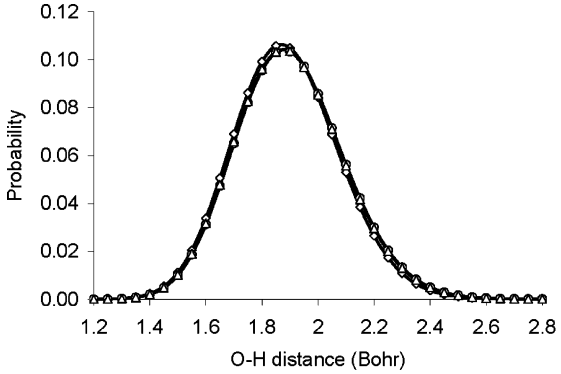

Figure 8. Example of PES convergence: convergence of the MP2/cc-pVDZ PES with respect to calculation of O−H wavefunction histograms for the hydrogen-bonded protons of monohydrated ethanediol. The wavefunction histograms were calculated from PES data sets comprised of 1 (◇), 75 (○), and 100 (△) unique data points. The standard error of the mean falls within the size of the data points.

surfaces, and these results are given in Tables 2 and 3, respectively.

All three potential energy surfaces predict qualitatively similar behavior of the protons, with the wavefunction histograms showing two proton environments. One proton environment corresponds to non-hydrogen-bonded protons, and the O−H wavefunction histogram for these protons is the same as that in gas-phase ethanediol (Figure 4). The other proton environment corresponds to hydrogen-bonded protons, where the wavefunction histogram is shifted to longer O−H distances, relative to the gas-phase. The shift of the wavefunction histogram to longer distance indicates proton delocalization, which is indicative of the presence of intermolecular hydrogen bonding. The main difference between the O−H wavefunction histograms is the extent of proton delocalization for the hydrogen-bonded protons; results obtained from the PW91 surface demonstrate a larger shift of the wavefunction histogram to long distance compared to those obtained from the B3LYP and MP2 surfaces. This effect can also be observed from the vibrationally averaged O−H distances (Table 2); B3LYP and MP2 predict a 0.023 Å shift to longer distance, whereas PW91 predicts a 0.043 Å shift.

From Table 3, we observe that all three surfaces predicted similar results for the vibrationally averaged O−O distances. The intramolecular O−O distance was found to be ~0.3 Å longer than the intermolecular O−O distances, for all methods considered. Together with the fact that the O−H distances and wavefunction histograms show no proton delocalization, the elongation of intramolecular O−O distances relative to the gas phase and intermolecular O−O distances provides conclusive evidence that there is no intramolecular hydrogen bonding in monohydrated 1,2-ethanediol. The intermolecular O−O distances were found to be around 2.75 Å, a distance consistent with the existence of weak hydrogen bonding. This is confirmed by the delocalization of the protons involved in intermolecular hydrogen bonding.

Conclusions

The extent of inter- and intramolecular hydrogen bonding in gas-phase and monohydrated 1,2-ethanediol has been determined by calculation of the nuclear vibrational wavefunction. Separate O−H wavefunction histograms were constructed for each O−H distance by projection of this wavefunction into bondlength coordinates. Each different O−H distance was distinguished by labeling the otherwise CNP-indistinguishable atoms. Analysis of the degree of proton delocalization, measured by a shift in the O−H wavefunction histogram, provides a sensitive and sensible means of quantifying the notion of hydrogen bonding. A number of questions have been specifically posed and addressed in this work, and the answers are summarized below.

(1) Does 1,2-ethanediol have an intramolecular hydrogen bond?

Maybe. The quantitative similarity between the O−H distribution functions for the terminal hydroxide and the putative hydrogen-bonded hydroxide is evidence of a lack of intramolecular hydrogen bonding. However, the resolution of the QDMC simulation is relatively low, and the vibrationally averaged O−O distances are consistent with the possibility of weak hydrogen bonding.

2. How is the intramolecular 1,2-ethanediol bonding changed upon the addition of a water molecule? Does monohydrated 1,2-ethanediol have an intramolecular hydrogen bond, only intermolecular hydrogen bonds, or both?

Monohydrated 1,2-ethanediol does not possess an intramolecular hydrogen bond. No change in the intramolecular O−H wavefunction is observed upon solvation, and indeed, the vibrationally averaged intermolecular O−O distance increases in monohydrated ethanediol with respect to gas-phase ethanediol. Monohydrated ethanediol does, on the other hand, possess two intermolecular hydrogen bonds, both of equal strength. This is evidenced by a shift of the O−H wavefunction histograms to longer distance, implying proton delocalization, and a relatively short vibrationally averaged O−O distance.

3. What is the effect of using different levels of ab initio theory to construct the global PES on the nuclear vibrational wave function, in particular, on the extent and nature of hydrogen bonding?

The treatment of electron correlation in the *ab initio* theory used to construct the PES has a significant effect on the calculated nuclear vibrational wavefunction. B3LYP and MP2 produce quantitatively similar results for both gas-phase and monohydrated ethanediol, whereas PW91 overestimates the vibrationally averaged O−H distances and the degree of proton delocalization due to hydrogen bonding relative to the B3LYP and MP2 results. In general, density functional methods should be benchmarked against higher-level *ab initio* methods for hydrogen-bonded systems.

References and Notes

(1) Radom, L.; Lathan, W. A.; Hehre, W. J.; Pople, J. A. *J. Am. Chem. Soc.* **1973**, *95*, 693−698.

(2) Ha, T. K.; Frei, H.; Meyer, R.; Günthard, H. H. *Theor. Chim. Acta* **1974**, *34*, 277.

(3) Almlöf, J.; Stymne, H. *Chem. Phys. Lett.* **1975**, *33*, 118−120.

(4) Frei, H.; Ha, T. K.; Meyer, R.; Günthard, H. H. *Chem. Phys.* **1977**, *25*, 271.

(5) Van Alsenoy, C.; Van Den Enden, L.; Schäfer, L. *THEOCHEM* **1984**, *108*, 121−128.

(6) Pople, J. A.; Head-Gordon, M.; Raghavachari, K. *J. Chem. Phys.* **1987**, *87*, 5968−5975.

(7) Cabral, B. J. C.; Albuquerque, L. M. P. C.; Fernandes, F. M. S. S. *Theor. Chim. Acta* **1991**, *78*, 271−280.

(8) Nagy, P. I.; Dunn, W. J.; Alagona, G.; Ghio, C. *J. Am. Chem. Soc.* **1991**, *113*, 6719−6729.

(9) Park, C. G.; Tasumi, M. *J. Phys. Chem.* **1991**, *95*, 2757−2762.

(10) Alagona, G.; Ghio, C. *THEOCHEM* **1992**, *254*, 287−300.

(11) Hooft, R. W. W.; van Eijck, B. P.; Kroon, J. *J. Chem. Phys.* **1992**, *97*, 3639−3646.

(12) Murcko, M. A.; DiPaola, R. A. *J. Am. Chem. Soc.* **1992**, *114*, 10010−10018.

(13) Nagy, P. I.; Dunn, W. J.; Alagona, G.; Ghio, C. *J. Am. Chem. Soc.* **1992**, *114*, 4752−4758.

(14) Carmichael, I.; Chipman, D. M.; Podlasek, C. A.; Serianni, A. S. *J. Am. Chem. Soc.* **1993**, *115*, 10863−10870.

(15) Cramer, C. J.; Truhlar, D. G. *J. Am. Chem. Soc.* **1994**, *116*, 3892−3900.

(16) Oie, T.; Topol, I. A.; Burt, S. K. *J. Phys. Chem.* **1994**, *98*, 1121−1128.

(17) Yeh, T.-S.; Chang, Y.-P.; Su, T.-M.; Chao, I. *J. Phys. Chem.* **1994**, *98*, 8921−8929.

(18) Bultinck, P.; Goeminne, A.; Van de Vondel, D. *THEOCHEM* **1995**, *357*, 19−32.

(19) Csonka, G. I.; Anh, N.; Ángyán, J.; Csizmadia, I. G. *Chem. Phys. Lett.* **1995**, *245*, 129−135.

(20) Csonka, G. I.; Csizmadia, I. G. *Chem. Phys. Lett.* **1995**, *243*, 419−428.

(21) Chang, Y.-P.; Su, T.-M.; Li, T.-W.; Chao, I. *J. Phys. Chem. A* **1997**, *101*, 6107−6117.

(22) Cabral, B. J. C. *Int. J. Quantum Chem.* **1998**, *60*, 1651−1660.

(23) Manivet, P.; Masella, M. *Chem. Phys. Lett.* **1998**, *288*, 642−646.

(24) Trindle, C.; Crum, P.; Douglass, K. *J. Phys. Chem. A* **2003**, *107*, 6236−6242.

(25) Mandado, M.; Grana, A.; Mosquera, R. *Phys. Chem. Chem. Phys.* **2004**, *6*, 4391−4396.

(26) Bastiansen, O. *Acta Chem. Scand.* **1949**, *3*, 415.

(27) Kuhn, L. P. *J. Am. Chem. Soc.* **1952**, *74*, 2492−2499.

(28) Krueger, P. J.; Mettee, H. D. *J. Mol. Spectrosc.* **1965**, *18*, 131.

(29) Buckley, P.; Giguère, P. A. *Can. J. Chem.* **1967**, *45*, 397.

(30) Pachler, K. G. R.; Wessels, P. L. *J. Mol. Struct.* **1970**, *6*, 471−478.

(31) Busfield, W. K.; Ennis, M. P.; McEwen, I. J. *Spectrochim. Acta* **1973**, *29*, 1259−1264.

(32) Maleknia, S.; Friedman, B. R.; Abedi, N.; Schwartz, M. *Spectrosc. Lett.* **1980**, *13*, 777.

(33) Walder, E.; Bauder, A.; Günthard, H. H. *Chem. Phys.* **1980**, *51*, 223−239.

(34) Caminati, W.; Corbelli, G. *J. Mol. Spectrosc.* **1981**, *90*, 572−578.

(35) Takeuchi, H.; Tasumi, M. *Chem. Phys.* **1983**, *77*, 21−34.

(36) Christen, D.; Coudert, L. H.; Larsson, J. A.; Cremer, D. *J. Mol. Spectrosc.* **2001**, *205*, 185−196.

(37) Klein, R. A. *J. Comput. Chem.* **2002**, *23*, 585.

(38) Koch, U.; Popelier, P. L. A. *J. Phys. Chem.* **1995**, *99*, 9747.

(39) Jordan, M. J. T.; Thompson, K. C.; Collins, M. A. *J. Chem. Phys.* **1995**, *102*, 5647.

(40) Thompson, K. C.; Jordan, M. J. T.; Collins, M. A. *J. Chem. Phys.* **1998**, *108*, 8302.

(41) Bettens, R. P. A.; Collins, M. A. *J. Chem. Phys.* **1999**, *111*, 816.

(42) Collins, M. A. *Theor. Chem. Acc.* **2002**, *108*, 313.

(43) Thompson, K. C.; Collins, M. A. *J. Chem. Soc., Faraday Trans.* **1997**, *93*, 871.

(44) Anderson, J. B. *J. Chem. Phys.* **1975**, *63*, 1499.

(45) Coker, D. F.; Watts, R. O. *Mol. Phys.* **1986**, *58*, 1113.

(46) Suhm, M. A.; Watts, R. O. *Phys. Rep.* **1991**, 293.

(47) Perdew, J. P. In *Electronic Structure of Solids '91*; Ziesche, P., Eschrig, H., Eds.; Akademie Verlag: Berlin, 1991.

(48) Perdew, J. P.; Chevary, J. A.; Vosko, S. H.; Jackson, K. A.; Pederson, M. R.; Singh, D. J.; Fiolhais, C. *Phys. Rev. B* **1992**, *46*, 6671.

(49) Perdew, J. P.; Chevary, J. A.; Vosko, S. H.; Jackson, K. A.; Pederson, M. R.; Singh, D. J.; Fiolhais, C. *Phys. Rev. B* **1993**, *48*, 4978.

(50) Perdew, J. P.; Burke, K.; Wang, Y. *Phys. Rev. B* **1996**, *54*, 16533.

(51) Burke, K.; Perdew, J. P.; Wang, Y. In *Electronic Density Functional Theory: Recent Progress and New Directions*; Dobson, J. F., Vignale, G., Das, M. P., Eds.; Plenum: New York, 1998.

(52) Lee, C.; Yang, W.; Parr, R. G. *Phys. Rev. B* **1988**, *37*, 785.

(53) Becke, A. D. *J. Chem. Phys.* **1993**, *98*, 5648.

(54) Møller, C.; Plesset, M. S. *Phys. Rev.* **1934**, *46*, 618.

(55) Woon, D. E.; Dunning, T. H., Jr. *J. Chem. Phys.* **1993**, *98*, 1358.

(56) Frisch, M. J.; Trucks, G. W.; Schlegel, H. B.; Scuseria, G. E.; Robb, M. A.; Cheeseman, J. R.; Montgomery, J. A., Jr.; Vreven, T.; Kudin, K. N.; Burant, J. C.; Millam, J. M.; Iyengar, S. S.; Tomasi, J.; Barone, V.; Mennucci, B.; Cossi, M.; Scalmani, G.; Rega, N.; Petersson, G. A.; Nakatsuji, H.; Hada, M.; Ehara, M.; Toyota, K.; Fukuda, R.; Hasegawa, J.; Ishida, M.; Nakajima, T.; Honda, Y.; Kitao, O.; Nakai, H.; Klene, M.; Li, X.; Knox, J. E.; Hratchian, H. P.; Cross, J. B.; Adamo, C.; Jaramillo, J.; Gomperts, R.; Stratmann, R. E.; Yazyev, O.; Austin, A. J.; Cammi, R.; Pomelli, C.; Ochterski, J. W.; Ayala, P. Y.; Morokuma, K.; Voth, G. A.; Salvador, P.; Dannenberg, J. J.; Zakrzewski, V. G.; Dapprich, S.; Daniels, A. D.; Strain, M. C.; Farkas, O.; Malick, D. K.; Rabuck, A. D.; Raghavachari, K.; Foresman, J. B.; Ortiz, J. V.; Cui, Q.; Baboul, A. G.; Clifford, S.; Cioslowski, J.; Stefanov, B. B.; Liu, G.; Liashenko, A.; Piskorz, P.; Komaromi, I.; Martin, R. L.; Fox, D. J.; Keith, T.; Al-Laham, M. A.; Peng, C. Y.; Nanayakkara, A.; Challacombe, M.; Gill, P. M. W.; Johnson, B.; Chen, W.; Wong, M. W.; Gonzalez, C.; Pople, J. A. *Gaussian 03*, revision C.02; Gaussian, Inc.: Pittsburgh, PA, 2003.

(57) Del Bene, J. E.; Jordan, M. J. T. *Int. Rev. Phys. Chem.* **1999**, *18*, 119−162.